Probabilistic Sweet Spots Predict Motor Outcome for Deep Brain Stimulation in Parkinson Disease

Till A. Dembek, MD,[1,2]* Jan Roediger,[1]* Andreas Horn, MD, PhD,[3] Paul Reker, MD,[1] Carina Oehrn, MD,[4] Haidar S. Dafsari, MD,[1] Ningfei Li,[3] Andrea A. Kühn, MD,[3] Gereon R. Fink, MD,[1,4] Veerle Visser-Vandewalle, MD,[2] Michael T. Barbe, MD,[1] and Lars Timmermann, MD[5]

Objective: To investigate whether functional sweet spots of deep brain stimulation (DBS) in the subthalamic nucleus (STN) can predict motor improvement in Parkinson disease (PD) patients.
Methods: Stimulation effects of 449 DBS settings in 21 PD patients were clinically and quantitatively assessed through standardized monopolar reviews and mapped into standard space. A sweet spot for best motor outcome was determined using voxelwise and nonparametric permutation statistics. Two independent cohorts were used to investigate whether stimulation overlap with the sweet spot could predict acute motor outcome (10 patients, 163 settings) and long-term overall Unified Parkinson's Disease Rating Scale Part III (UPDRS-III) improvement (63 patients).
Results: Significant clusters for suppression of rigidity and akinesia, as well as for overall motor improvement, resided around the dorsolateral border of the STN. Overlap of the volume of tissue activated with the sweet spot for overall motor improvement explained R^2 = 37% of the variance in acute motor improvement, more than triple what was explained by overlap with the STN (R^2 = 9%) and its sensorimotor subpart (R^2 = 10%). In the second independent cohort, sweet spot overlap explained R^2 = 20% of the variance in long-term UPDRS-III improvement, which was equivalent to the variance explained by overlap with the STN (R^2 = 21%) and sensorimotor STN (R^2 = 19%).
Interpretation: This study is the first to predict clinical improvement of parkinsonian motor symptoms across cohorts based on local DBS effects only. The new approach revealed a distinct sweet spot for STN DBS in PD. Stimulation overlap with the sweet spot can predict short- and long-term motor outcome and may be used to guide DBS programming.

ANN NEUROL 2019;86:527–538

Deep brain stimulation (DBS) of the subthalamic nucleus (STN) is an established therapeutic option in advanced Parkinson disease (PD). STN DBS has been shown to improve motor function and reduce motor fluctuations as well as medication intake.[1] However, the optimal stimulation target remains a matter of debate, as surveys among DBS specialists have demonstrated.[2] Studies investigating the locations of active contacts suggested different optimal positions inside the STN[3–6] or dorsomedial to it.[7] A systematic review of active contact locations found that only a minority were located inside the STN.[8] However, investigating contact locations only neglects differences in stimulation parameters and the spread of electrical stimulation, the so-called volume of tissue activated (VTA). Different approaches have been developed to estimate the spatial extent of the VTA.[9–13] Furthermore, VTAs have been used to determine the anatomical origins of DBS effects at an individual patient level.[14–17] So far, only a few

View this article online at wileyonlinelibrary.com. DOI: 10.1002/ana.25567

Received Aug 23, 2018, and in revised form Jul 7, 2019. Accepted for publication Jul 28, 2019.

Address correspondence to Dr Dembek, Department of Neurology, University Hospital of Cologne, Kerpener Straße 62, D-50934 Cologne, Germany. E-mail: till.dembek@uk-koeln.de

*T.A.D. and J.R. contributed equally.

From the [1]Department of Neurology, Faculty of Medicine, University of Cologne, Cologne; [2]Department of Stereotactic and Functional Neurosurgery, Faculty of Medicine, University of Cologne, Cologne; [3]Movement Disorders and Neuromodulation Unit, Department for Neurology, Charité–University Medicine Berlin, Berlin; [4]Cognitive Neuroscience, Institute of Neuroscience and Medicine, Jülich Research Center, Jülich; and [5]Department of Neurology, University Hospital of Marburg and Gießen, Marburg, Germany

studies have tried pooling data on stimulation location and clinical outcome over multiple subjects using probabilistic stimulation mapping. Probabilistic stimulation maps (PSMs) were created based on contact locations[18,19] or VTAs[20–26] for different DBS targets and indications. For PD and STN DBS, Butson et al created PSMs from a sample of n = 6 patients for bradykinesia and rigidity, which showed the highest improvement dorsal to the STN.[20] Yet, no further statistical verification was performed. Addressing this, Eisenstein et al introduced voxel-based statistics to verify their coordinate-based PSMs for STN DBS and found general improvement of motor symptoms in the STN and its surroundings.[18,19] Akram et al used a different statistical approach and found that the best locations for the improvement of akinesia, tremor, and rigidity were in different parts of the dorsal STN.[25] PSMs have been proposed to guide clinical programming in DBS[23] and could be used to establish imaging-based, semiautomated DBS programming algorithms.[27] However, to guide programming, the optimal stimulation "sweet spot" that most reliably predicts favorable clinical outcome needs to be known. We here aimed to identify such sweet spots for different PD motor symptoms. Based on previous work,[21] a novel pipeline for creating and validating PSMs was applied to a large dataset of prospective monopolar reviews of PD patients. We then used 2 independent test cohorts to investigate whether stimulation overlap with the identified sweet spot was able to predict acute and chronic motor improvement.

Patients and Methods

Ethics

This investigator-initiated study was approved by the ethics committee of the University of Cologne (Study Nos 14-337, 15-357) and conducted in accordance with the Declaration of Helsinki. Patients gave written informed consent before study participation.

Data Acquisition

PSM Creation Dataset. Twenty-one PD patients who had received DBS in the STN at the University Hospital Cologne were recruited for this study. Inclusion criteria were the clinical diagnosis of PD without severe cognitive impairment or significant neuropsychiatric problems, a significant L-dopa and stimulation response, a minimum of 3 months elapsed since DBS surgery, and the ability to undergo an extended monopolar review of approximately 3 hours after overnight withdrawal of dopaminergic medication. During recruitment, normal impedance levels were ensured and the DBS device was turned off to identify the upper extremity more severely affected by motor symptoms. The lead contralateral to the predominantly affected body side was examined while the other lead was left on its clinical DBS setting to reduce patient discomfort and increase compliance during the assessment. Five patients agreed to repeat the monopolar review on the less affected hemisphere the following day, while maintaining withdrawal of dopaminergic medication.

During the monopolar reviews, contacts were interrogated by increasing stimulation amplitudes in 1mA steps to a maximum of 5mA or until persistent (>1 minute) or intolerable side effects occurred. Pulse width was set to 60 microseconds and frequency to 130Hz in all patients. Contacts were interrogated in randomized order with the patient being unaware of which contact was active. If no side effects occurred in a stimulation setting, instructions for movement tasks were given via standardized videos. Symptom severity of rigidity, akinesia, resting tremor, and postural tremor of the contralateral arm was assessed by the same rater (J.R.). Rigidity was assessed according to item 22 of the Unified Parkinson's Disease Rating Scale (UPDRS) Part III. For tremor, the mean of 2 UPDRS items was assessed (item 20, rest tremor; item 21, postural tremor). Severity of akinesia was assessed using the mean of items 23 (finger tapping) and 25 (hand rotation). Additional half-point steps were allowed to increase the resolution of the rating.[28] Additionally, tremor and akinesia were quantified by calculating the total travel distance during the abovementioned tasks using a motion tracking system (CMS 20; Zebris Medical, Isny, Germany).[28] These quantitative results were analyzed separately from the clinical ratings. Baseline symptom severity (DBS off) was reassessed before beginning stimulation on each contact. For each stimulation setting, the motor improvement was calculated by subtracting the average baseline score. Occurrence of side effects was rated from 0 to 3, reflecting no, slight, moderate, or severe appearance during stimulation. If a limiting side effect occurred at stimulation amplitudes <5mA and testing had to be aborted, we assumed that the same side effect would also have occurred during stimulation with the higher amplitudes not tested. If a patient did not show a specific motor symptom at baseline, they were excluded from the analysis of this symptom. In addition to the separate symptoms, we also calculated the *overall motor improvement* by averaging clinical improvements of rigidity, akinesia, and tremor. We further calculated a score for the occurrence of *any side effect* by pooling the data from all separate side effects.

Test Dataset 1. The first test dataset consisted of 10 PD patients who had received bilateral STN DBS at the University Hospital Cologne with directional DBS leads (Cartesia; Boston Scientific, Marlborough, MA). Patient characteristics of this dataset have been published previously.[28] In brief, patients underwent a monopolar review

on both hemispheres, with the 3 directional contacts on the clinically best directional level in each hemisphere being investigated with increasing amplitudes up to 5mA. Motor tasks and assessment were conducted similarly to the ones explained above, but clinical ratings were double-blind, as neither patient nor rater knew which contact was activated. In total, the dataset consisted of 163 individual stimulation settings. Overall motor improvement was again assessed by averaging the improvements of rigidity, akinesia, and tremor.

Test Dataset 2. The second test dataset consisted of 63 PD patients who had received bilateral STN DBS at Charité–University Medicine Berlin (n = 51) or the University Hospital Cologne (n = 12). The Berlin dataset has been published previously and consisted of different subcohorts whose data were collected in the course of different prospective DBS trials or from patient files.[29,30] The Cologne dataset was collected as part of a prospective DBS registry. For each patient, UPDRS-III motor scores were obtained in the medication OFF condition both preoperatively and at least 6 months postoperatively with clinical DBS settings.

Data Analyis

Lead Localization and Standardization

Image processing and lead localization were performed using the Lead-DBS toolbox (https://www.lead-dbs.org/).[30] Preoperative magnetic resonance imaging (MRI) and postoperative computed tomographic images were coregistered linearly using Advanced Normalization Tools (ANTs).[31] Images were then normalized into the Montreal Neurological Institute (MNI) space (2009b, nonlinear, asymmetric) using the symmetric diffeomorphic registration approach (SyN) implemented in ANTs and the "subcortical refine" setting as implemented in Lead-DBS.[31–33] Lead trajectories were identified using the PaCER algorithm.[34] For directional leads, the rotation was confirmed using the DiODe algorithm.[35] For the Berlin cohort, image coregistration and lead localization were performed using SPM12 and the TRAC/CORE algorithms, because a majority of patients had postoperative MRI scans.[30] All steps were visually inspected to ensure data quality.

Volume of Tissue Activated. VTAs were calculated using a finite element method approach as implemented in Lead-DBS.[29] Anisotropic conductivity values for gray (σ = 0.33S/m) and white matter (σ = 0.14S/m) were chosen. The electric field threshold was set to e = 0.2V/mm, which approximates the VTA radius estimate by Mädler and Coenen.[9,11,29]

Probabilistic Stimulation Maps. PSMs were created for each symptom (rigidity, akinesia, and tremor) and each encountered side effect separately as well as for the combined overall motor improvement and the occurrence of any side effect. For each examined stimulation setting, the respective VTA was created. Left hemispheric VTAs were nonlinearly flipped to the right hemisphere using Lead-DBS. Then all VTAs were transferred to the same $40 \times 40 \times 40$mm template space covering the wider STN area. The spatial resolution was set to 0.5mm, the same as the MNI template. Each voxel of the VTA was then assigned the clinical outcome during stimulation. Then, all VTAs were pooled across subjects, and the numbers of contributing VTAs, as well as their mean clinical outcome, were obtained for each voxel, resulting in the *N-image* and the *Mean-image*.

Voxel-Based Statistical Analysis. For further statistical analysis, voxels with less than n = 16 inputs were discarded.[21] This threshold was chosen as it allows for statistical approximation of the Wilcoxon signed rank test (see below) and it results in each voxel having to receive input from at least 4 different contacts. To statistically investigate the outcomes in each voxel, they had to be compared against a meaningful null hypothesis H_0. Previous studies used zero change ($H_0 = 0$) as their null hypothesis.[18,19,21] In STN DBS, however, some improvement in motor symptoms is seen on most contacts and a worsening of symptoms occurs only very rarely. Testing against $H_0 = 0$ thus results in almost all voxels showing statistically significant improvement.[19,21] We therefore chose a more conservative approach, which was that the null hypothesis should reflect the average stimulation outcome one would expect if the outcome was solely dependent on the stimulation amplitude and independent of stimulation location. This was represented in the *H_0-image* by calculating the average improvement at all 5 stimulation amplitudes and assigning each VTA not its original outcome value, but the average outcome of its stimulation amplitude. For example, all 1mA VTAs were assigned the average symptom improvement at 1mA. Therefore, the resulting *H_0-image* accounts for the fact that voxels that are being stimulated by higher amplitude VTAs can be expected to be associated with greater symptom improvement. We then could statistically test each voxel's original outcomes in the *Mean-image* against the expected outcomes in the *H_0-image* using a Wilcoxon signed rank test. After subtracting the *H_0-image* from the *Mean-image*, we identified all voxels that showed significant ($p < 0.05$) positive outcomes (higher symptom suppression or more side effects) and discarded all remaining voxels from further analysis.

Nonparametric Permutation Analysis. As in all voxel-based statistics, there is an increased risk of type 1 errors due to multiple comparisons. Additionally, our monopolar dataset consists of a variety of observations from the same leads and contacts, which are not independent from one another. To address these problems, we performed a nonparametric cluster-based permutation analysis comparing the results of our voxel-based analysis (ie, *Mean-image* vs *H_0-image*) to surrogate datasets. Following an approach proposed by Eisenstein et al,[18] we first created 1,000 *Permuted-mean-images*.[21] To do so, we shuffled the leads and the order of contacts within each lead, thus maintaining the grouping of contacts within each lead during the permutations (Fig 1B). Analogous to the analysis steps of the original dataset, *Permuted-mean-images* were generated pooling all of the newly assigned VTAs and then tested against the *H_0-image*. Next, clusters of significant voxels were identified in the original and the permuted datasets. A significant voxel belonged to a cluster if all its direct neighbors were also significant. For each cluster, we calculated a summary statistic to assess its overall validity. The cluster's summary statistic was the sum of the negative decadic logarithm of the p values of its voxels.[18,19,21] Because large clusters with highly significant voxels are unlikely to exist by chance alone, noncoincidental clusters from the original dataset should yield greater summary statistics than clusters from the permuted datasets. Hence, we ranked the summary statistics of our original clusters within the permutation distribution of the summary statistics of the permuted clusters. All clusters with summary statistics <95% of the permuted summary statistics were discarded. In other words, only clusters with a p value <0.05 within the permutation distribution were accepted as valid sweet spots for either symptom suppression or side effects. Figure 1 provides an overview of the methodology.

Test Dataset Validation. To validate our sweet spot for overall motor improvement, we aimed at predicting DBS motor response in the 2 independent test cohorts based on stimulation overlap to the sweet spot. Using the first test cohort, we investigated whether our sweet spot could predict acute motor outcome observed during monopolar reviews. For each stimulation setting, we therefore calculated the percentage of the sweet spot that was covered by the corresponding VTA. We then used linear mixed-effect models to determine to what extent this overlap could predict symptom improvement, while accounting for non-independence of stimulation effects within individual leads. Overlap was therefore introduced as a fixed effect and the association to a particular lead as a random effect. To compare the predictive quality of the sweet spots to other neuroanatomical structures, we also repeated the linear mixed-effect model analysis using the VTAs' overlap

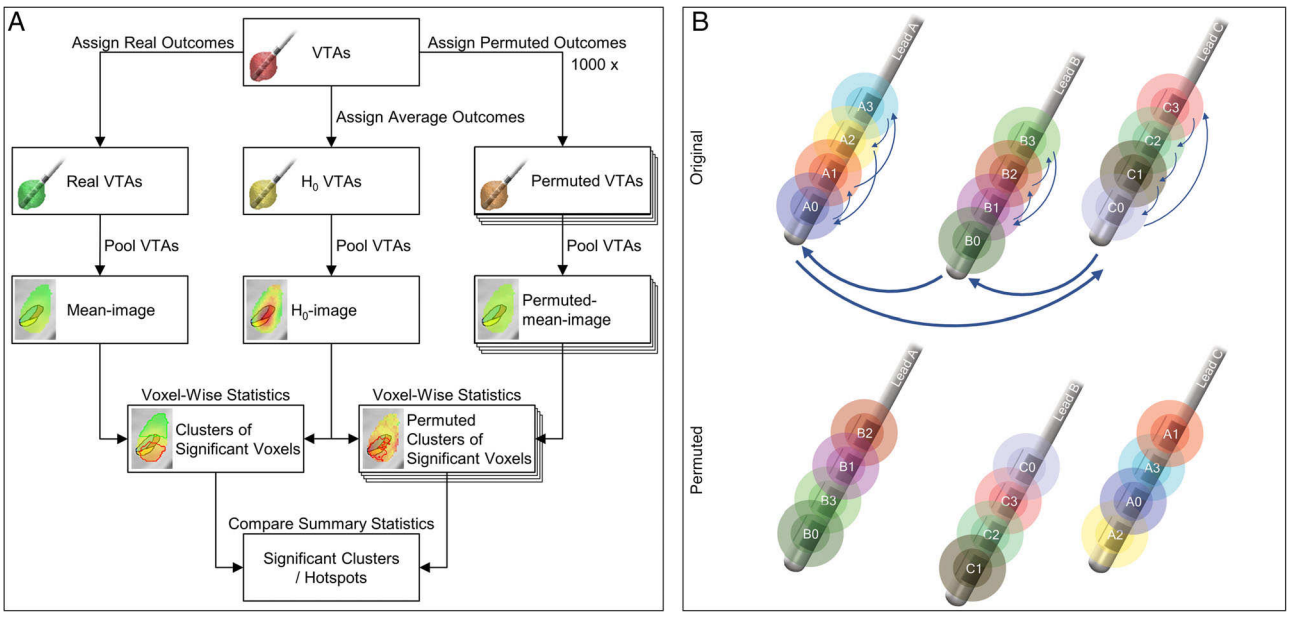

FIGURE 1: (A) Schematic overview of the statistical analysis. Each volume of tissue activated (VTA) was either assigned its outcome (left), the average outcome at its stimulation amplitude (center), or a permuted outcome from another lead at the same amplitude (right). Pooling all VTAs then resulted in the *Mean-image*, the *H_0-image*, or a *Permuted-mean-image*, respectively. Outcomes at each voxel of the *Mean-images* were statistically compared to the *H_0-image*. Finally, summary statistics of clusters of significant voxels in the *Mean-image* were compared to those of the *Permuted-mean-images* to determine the overall significant clusters. (B) Schematic overview of the permutation scheme. VTAs from the same contact stayed together, but contacts were randomly reordered within the lead and reassigned to the position of a different lead.

with the STN and the sensorimotor STN[36] as predictors of clinical outcomes. Models are described using the amount of variance R^2 explained by the fixed effect, the p value of the fixed effect, and the Akaike information criterion (AIC; smaller values indicating better model fit; differences >2 indicating model superiority of the model with the lower AIC).[37] Using the second test dataset, we also aimed at investigating whether our sweet spot could predict the overall UPDRS-III motor outcome of chronic DBS settings. Again, the VTA overlap with the sweet spot, as well as the STN and the sensorimotor STN, was calculated. Because patients were stimulated bilaterally, the sum of the overlaps of both hemispheres was calculated. We then used a linear regression model to investigate whether this bilateral overlap could predict improvement on the UPDRS-III.

Post Hoc Analysis. In an additional analysis, we also compared our sweet spot for overall motor improvement to previously published results. To make our sweet spot volume comparable to previously published coordinates,[5,6,8,25] we calculated its center of mass.

Technical Realization. All calculations were performed in MATLAB R2018a (MathWorks, Natick, MA).

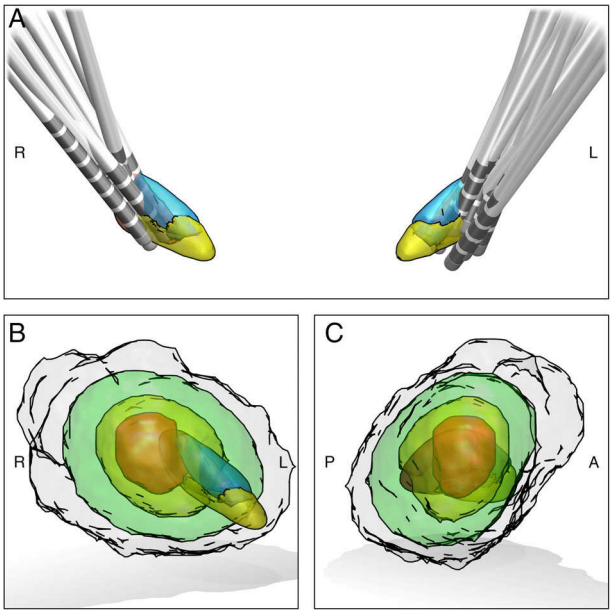

FIGURE 2: (A) Lead locations of the probabilistic stimulation map creation dataset (n = 26) seen from anterior together with tripartite subthalamic nuclei (dark red = sensorimotor, blue = associative, yellow = limbic).[36] (B) Anterior and (C) lateral views depicting how often voxels were stimulated. Colored volumes reflect stimulation by n ≥ 1 (gray), n ≥ 16 (green, threshold for voxel-based statistics), n ≥ 100 (yellow), and n ≥ 200 VTAs (red). A = anterior; L = left; P = posterior; R = right.

Results

PSM Creation Cohort

A total of 449 stimulation settings on 26 leads and 99 contacts were used to create PSMs. The assessment of 3 leads had to be aborted due to patient fatigue, but fully investigated contacts were still included in the dataset. Figure 2 displays lead locations and the *N-image*. The *N-image* and thus the volume analyzed in this study covered most of the STN and its surroundings.

Motor Symptoms

PSMs were created for overall motor improvement, the clinical and the quantitative assessments of akinesia and tremor, and for rigidity. For overall motor improvement (p = 0.009), as well as for rigidity (p = 0.001) and akinesia (clinical: p = 0.017; quantitative: p = 0.009), one cluster with above average symptom suppression remained significant after nonparametric permutation analysis. Several smaller clusters were rejected (Table 1). Tremor clusters did not reach significance (clinical: p = 0.66; quantitative: p = 0.72). The sweet spot for overall motor improvement was centered on the dorsolateral STN and covered the dorsal parts of both the atlas-defined sensorimotor STN and the associative STN as well as the surrounding white matter. The significant clusters for clinical improvements of rigidity and akinesia showed a similar distribution. The cluster for quantitative improvement of akinesia was smaller than the one for clinical improvement, but 89% of its volume overlapped with the clinical cluster. Figure 3 provides a direct comparison of the *Mean-images* and the significant clusters for all motor symptoms. Overlaps with the STN are presented in Table 1 for all significant clusters.

Side Effects

Side effects occurred in 60 of 449 examined settings. A variety of side effects were encountered, with dysarthria being the most common (n = 26), followed by muscle contractions (n = 23), disturbed vision (n = 17), dizziness (n = 16), paresthesia (n = 13), and mood changes (n = 10). None of the clusters for individual side effects reached statistical significance (see Table 1). For the occurrence of *any side effect*, a significant cluster was found that covered parts of the posteroventral STN and much of its posteroventral surroundings (see Fig 3).

Predicting Acute Motor Outcome

The first independent test cohort, consisting of 10 patients with a total of 163 directional DBS settings, was used to investigate the predictive value of the sweet spot for overall motor improvement to predict acute motor outcome and whether sweet spot–based predictions were more accurate compared to those based on the STN and sensorimotor

TABLE 1. Number of Clusters Discarded after Nonparametric Permutation Statistics as Well as Statistics of Significant Clusters

Symptoms	Discarded Clusters	Significant Clusters	Rank	*p*	Size	Inside STN	Inside Sensorimotor STN
Overall motor improvement	4	1	991	0.009[a]	359mm^3	20%	11%
Rigidity	1	1	999	0.001[a]	420mm^3	24%	12%
Akinesia, clinical rating	1	1	983	0.017[a]	282mm^3	15%	11%
Akinesia, quantitative	13	1	991	0.009[a]	111mm^3	9%	10%
Tremor, clinical rating	10	0	340	0.66			
Tremor, quantitative	3	0	278	0.722			
Side effects							
Any side effect	3	1	999	0.001[a]	194mm^3	11%	7%
Dysarthria	2	0	373	0.627			
Muscle contractions	6	0	516	0.484			
Paresthesia	5	0	820	0.18			
Mood changes	4	0	686	0.314			
Visual disturbance	10	0	311	0.689			
Dizziness	15	0	202	0.798			

[a]Statistically significant.
STN = subthalamic nucleus.

STN (Fig 4). We therefore calculated 3 linear mixed-effect models introducing VTA overlap with the overall sweet spot, the whole STN, and the sensorimotor STN as fixed effect, while accounting for individual leads as a random effect. Although overlap as the fixed effect was significant in all models, both the amount of variance explained by the fixed effect (R^2) and the AIC revealed that the model using overlap with the sweet spot (R^2 = 37%, $p < 10^{-9}$, AIC = −79.8) clearly outperformed overlap with the STN (R^2 = 9%, $p < 10^{-6}$, AIC = −54.0) and its sensorimotor subpart (R^2 = 10%, $p < 10^{-7}$, AIC = −45.8). Notably, significant leadwise random effects only occurred in 4 of 20 leads and in all individual leads the relation between sweet spot overlap and outcome was positive.

Predicting Chronic Motor Outcome

For the second independent test cohort, consisting of 63 patients, overlaps were used to predict total UPDRS-III improvement (Fig 5). Again, overlap was a significant predictor in all models and stimulation overlap with the sweet spot explained R^2 = 20% ($p < 10^{-3}$, AIC = 0.9) of the variance in UPDRS-III improvement, whereas overlap with the sensorimotor STN explained R^2 = 19% ($p < 10^{-3}$, AIC = 1.5) and overlap with the whole STN explained R^2 = 21% (AIC = 0.1, $p < 10^{-3}$). Both R^2 and AIC revealed no relevant differences between models.

Comparison to Other Sweet Spots

The center of mass of the sweet spot was x = 12.50mm, y = −12.72mm, z = −5.38mm for the right hemisphere (MNI coordinates). The distance to the sweet spot coordinate from Horn et al[5] and Caire et al[8] was only 0.56mm, and both sweet spots were positioned at the dorsal interface between sensorimotor and associative STN. The sweet spot published by Bot et al[6] was slightly anterior and had a distance of 1.34mm to our sweet spot. On the other hand, the sweet spot by Akram et al[25] was positioned 2.41mm more ventral and medial to our sweet spot, again at the interface between sensorimotor and associative STN. A comparison of the sweet spots is shown in Figure 6; coordinates can be found in Table 2.

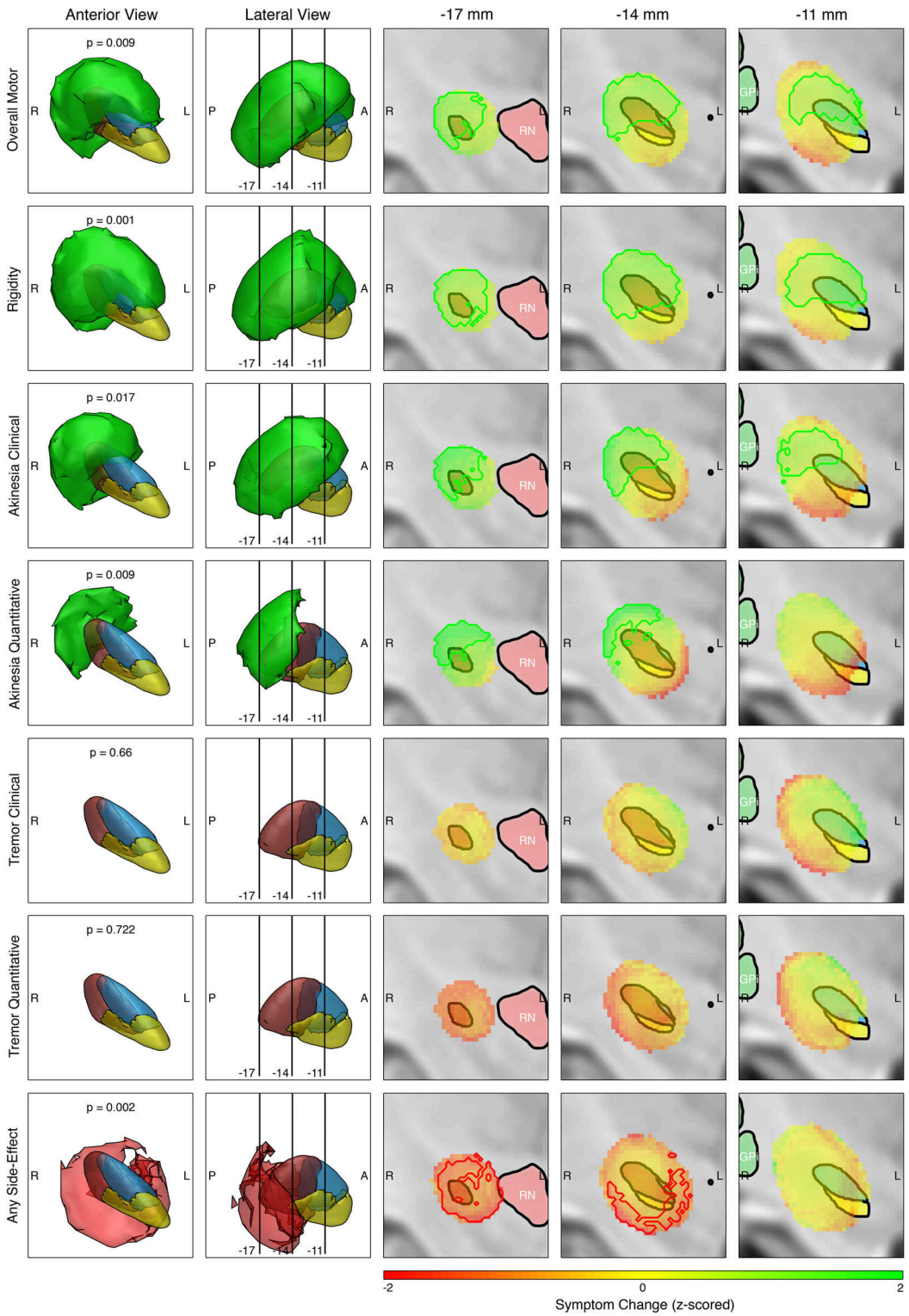

FIGURE 3: Probabilistic stimulation maps and significant clusters for different motor symptoms and the occurrence of side effects. The first 2 columns show significant clusters with good improvement (green) or high side effect occurrence (red, last row) from anterior (1st column) and lateral (2nd column) together with a tripartite subthalamic nucleus (sensorimotor = dark red, associative = blue, limbic = yellow). The remaining columns depict coronal slices through the *Mean-image* at y = −17/−14/−11mm. To compare clinical and quantitative symptom assessments, improvement was *z*-scored and is color-coded according to the colorbar. Outlines of the significant clusters are again shown in green/red. All atlas structures are based on the DISTAL atlas.[36] A = anterior; GPi = globus pallidus internus; L = left; P = posterior; R = right; RN = red nucleus.

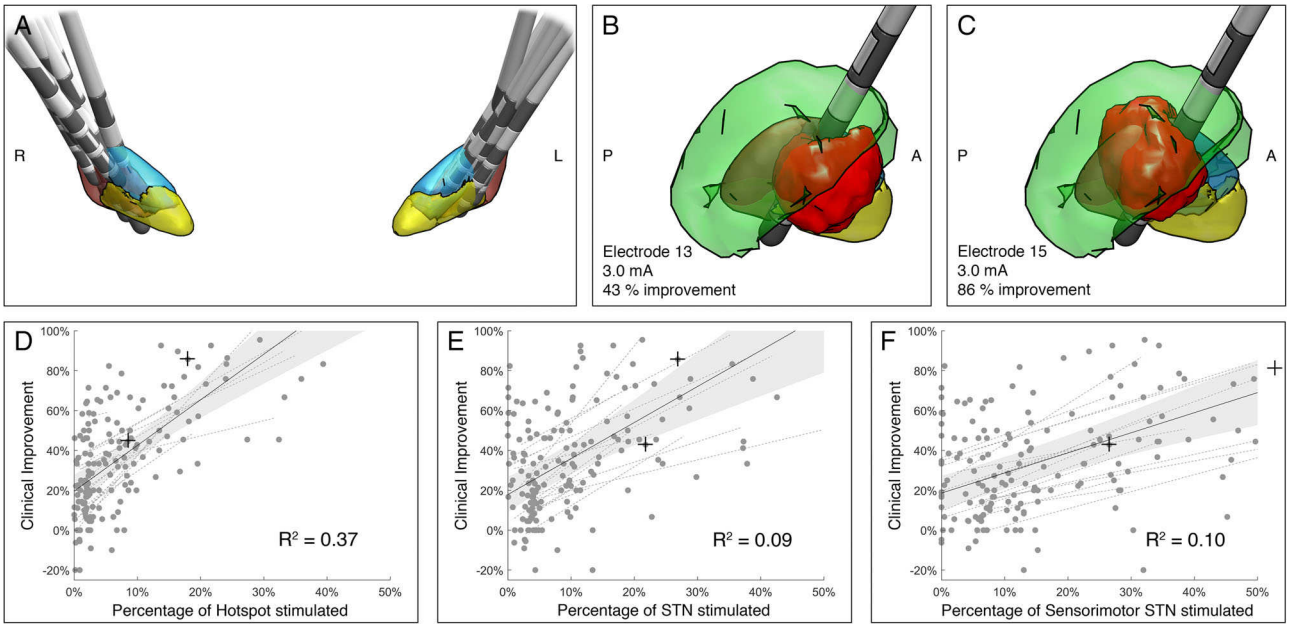

FIGURE 4: (A) Lead locations of test dataset 1 (n = 20), together with tripartite subthalamic nuclei (STN; dark red = sensorimotor, blue = associative, yellow = limbic). (B, C) Lateral views of an example patient (Patient 7) with directional volumes of tissue activated (VTAs; red) at 3mA amplitudes on contacts 13 and 15 shown together with the sweet spot for overall motor improvement (green). Stimulation at contact 15 showed much larger overlap with the sweet spot and better acute motor improvement. (D–F) Linear mixed-effect model (black) and 95% confidence interval (gray) between acute motor improvement and the percentage of the sweet spot (D), the STN (E), and the sensorimotor STN (F) covered by the respective VTA. Random effects for each individual hemisphere are also shown (dashed, gray). Stimulation overlap with the sweet spot explained more than triple the variance compared to overlap with the STN or the sensorimotor STN. Plus signs mark the stimulation settings from B and C. A = anterior; L = left; P = posterior; R = right.

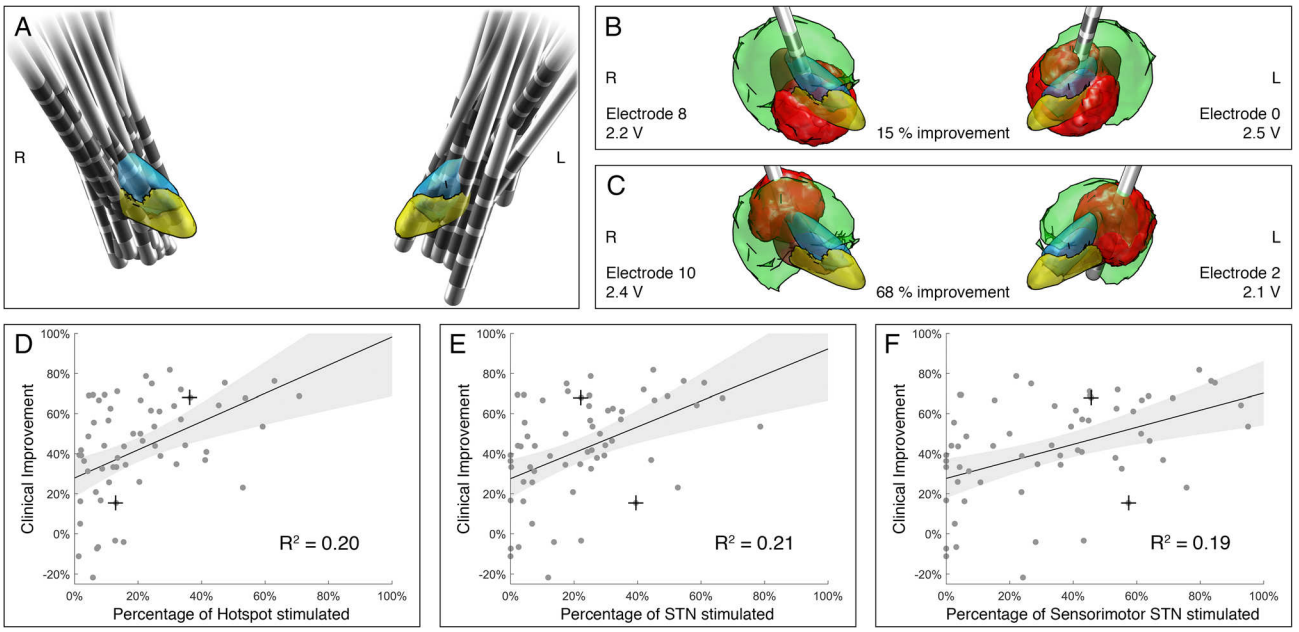

FIGURE 5: (A) Lead locations of test dataset 2 (n = 126), together with tripartite subthalamic nuclei (STNs; dark red = sensorimotor, blue = associative, yellow = limbic). (B, C) Anterior views of volumes of tissue activated (VTAs; red) with amplitudes of Patient 8 (B) and Patient 29 (C) shown together with the sweet spot for overall motor improvement (green). (D–F) Linear regression (black) and 95% confidence interval (gray) between chronic motor improvement and the percentage of the sweet spot (D), the STN (E), and the sensorimotor STN (F) covered by the respective VTAs. Overlaps with the sweet spot, STN, and sensorimotor STN explained a comparable amount of variance in chronic motor improvement. Plus signs mark the stimulation settings from B and C. L = left; R = right.

Discussion

In this study, we determined and validated distinct spatial clusters for the suppression of akinesia, rigidity, and overall motor improvement from clinical data generated during prospective monopolar reviews. Stimulation overlap with the sweet spot for overall motor improvement was able to predict acute and chronic motor outcome in 2 independent cohorts.

Motor Symptoms

Significant clusters for the suppression of rigidity, akinesia, and overall motor improvement showed substantial overlap and covered parts of the (dorsolateral) STN. However, the majority of their volume lay outside the STN's border, which is in line with previous studies[8,20] but contradictory to others.[25] Although the PSMs for clinical and quantitative improvement of tremor showed a gradient toward better improvement dorsomedial of the STN, no cluster reached statistical significance (see Fig 3). The reason for this is most likely that many patients in our cohort did not experience tremor at baseline, and thus too few data existed to result in robust clusters. In addition to the clinical ratings, we performed a quantitative motion analysis for akinesia and tremor. The akinesia sweet spot found via quantitative analysis showed remarkable consistency with the one generated from clinical ratings. The quantitative analysis of tremor did not reveal a significant sweet spot, which was again consistent with the results from clinical ratings. This convergence not only substantiates the validity of the clusters found but also underlines the scale-independence of the approach. Our results suggest that both rigidity and akinesia share a common sweet spot, whereas it remains unclear whether this is also true for tremor. Importantly, we were able to use our sweet spot to predict clinical outcome in 2 independent cohorts. We successfully predicted acute motor improvement in an independent cohort that had been implanted with different, directional DBS leads and had received prospective monopolar reviews using a similar study design. These predictions were much more accurate than predictions based on the STN or the sensorimotor STN and explained more than triple the amount of variance in clinical outcome. When predicting differences in chronic and interindividual UPDRS-III improvement, however, overlap with the STN, the sensorimotor STN, or our sweet spot were equally effective and the overall amount of explained variance was lower. These results highlight 3 important points. First, there are differences between acute and chronic outcomes and attempts to predict one via the other may be more challenging than to predict one via the same. Second, chronic, and more importantly interindividual, outcome is a more complex endpoint with many contributing factors such as age, disease duration, and axial symptoms that possibly need to be taken into account when trying to explain interindividual variance.[29] Third, center-specific differences in surgical targeting might reduce the predictive capabilities of the Cologne-based sweet spot for the largely Berlin-based second test dataset. Large, multicenter datasets should be aggregated when determining sweet spots in the future. Different approaches to predicting DBS outcome in PD have been put forward in the past. A previous approach to predict stimulation outcome based solely on contact locations was unsuccessful.[38] Bot et al, on the other hand, found a negative correlation between UPDRS-III improvement and distance to a sweet spot they calculated from contact locations.[6] Horn et al were able to predict long-term UPDRS-III improvement based on structural and functional connectivity profiles.[29] Akram et al found that structural connectivity to the supplementary motor area predicted acute improvement in rigidity and akinesia, and connectivity to the primary motor cortex predicted tremor suppression.[25] Due to differences in data and statistics, it is, however, difficult to directly compare their results to ours.[25]

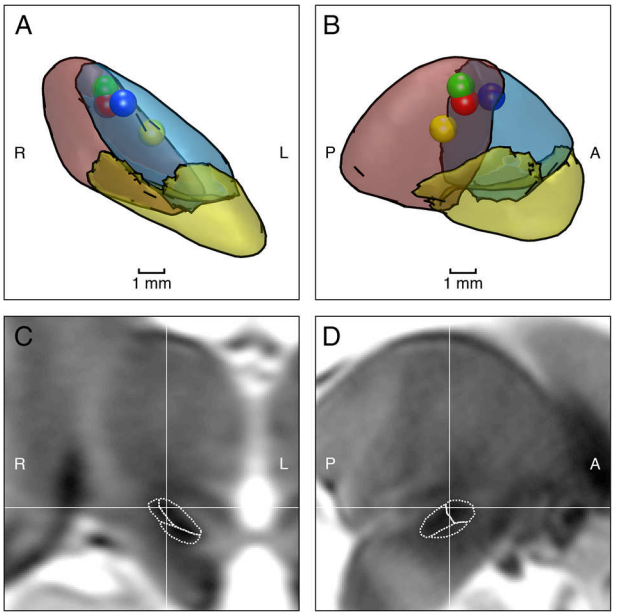

FIGURE 6: (A, B) Comparison of different sweet spots. The center of mass of the sweet spot for overall motor improvement from this study (green) is shown together with previously published sweet spots from Caire et al[5,8] (red), Bot et al[6] (blue), and Akram et al[25] (yellow). Whereas the center of our sweet spot as well as the sweet spots by Caire et al and Bot et al were positioned at the dorsal interface between sensorimotor STN (dark red) and associative STN (light blue), the sweet spot published by Akram et al. was slightly more ventral and medial. (C, D) Coronal and sagittal positions of the center of mass of our sweet spot in the Montreal Neurological Institute T2 template. A = anterior; L = left; P = posterior; R = right.

TABLE 2. Montreal Neurological Institute Coordinates of the Center of Mass of Our Sweet Spot for Overall Motor Improvement and Comparison to Other, Previously Published Sweet Spots

	x	y	z	Distance to Sweet Spot
Right hemisphere				
Sweet spot, center of mass	12.50mm	−12.72mm	−5.38mm	
Horn et al,[5] Caire et al[8]	12.42mm	−12.58mm	−5.92mm	0.56mm
Bot et al[6]	11.83mm	−11.63mm	−5.80mm	1.34mm
Akram et al[25]	10.83mm	−13.31mm	−7.01mm	2.41mm
Left hemisphere				
Sweet spot, center of mass	−12.68mm	−13.53mm	−5.38mm	
Horn et al,[5] Caire et al[8]	−12.58mm	−13.41mm	−5.87mm	0.52mm
Bot et al[6]	−12.02mm	−12.46mm	−5.78mm	1.32mm
Akram et al[25]	−11.00mm	−14.00mm	−7.00mm	2.38mm

Side Effects

Our analysis revealed that side effects in general were more likely to occur when stimulation was more posterior and more ventral. When mapping individual side effects, clusters did not reach statistical significance, most likely due to the small number of VTAs that were associated with side effects.

Methodological Considerations and Limitations

Different aspects should be considered regarding this study. First, we provide a statistical method to create voxel-based probabilistic stimulation maps for large DBS datasets that is especially suited but not limited to monopolar review data. The main novelty of our statistical approach is its more conservative null hypothesis formulated in the H_0*-image*. Compared to previous studies, this method ensures that only those voxels were identified that show statistically significant deviations from what one would expect to be a voxel's average stimulation outcome.[18,19,21] Another very important issue is that data from the same monopolar review have to be considered as dependent from one another. We addressed this problem by maintaining these dependencies in our nonparametric permutation analysis. Applying our nonparametric permutation analysis on spatial clusters of significant voxels instead of individual significant voxels furthermore reduces the risk of single false-positive voxels. Notably, we did not perform an additional correction for multiple comparisons regarding the number of investigated clinical and quantitative scores. On the other hand, most results would have withstood even rigorous Bonferroni correction (see Table 1) and the consistency of simultaneous clinical and quantitative scores further supports the validity of our results. VTA models more complex than the one used in our study have been proposed in the past. Different axon properties or axon orientations have been shown to influence activation in modeling studies.[11,39–41] However, most of the underlying properties are unknown, which is why we chose a model based on clinically observed thresholds and previously published results.[9,11,29] Although our dataset consisted of prospective, standardized monopolar reviews with >400 stimulation settings and both clinical and quantitative assessments, it was still limited to data from 21 patients. However, we validate findings on 73 additional out-of-sample patients with both short- and long-term effects. Larger datasets, preferably from multicenter cohorts, could help to improve sweet spot generation and possibly increase predictive capabilities.

Neuroanatomical Implications

In recent years, the scientific focus regarding target structures of DBS has shifted from nuclei to fiber tracts.[29,42] Our results are in line with this development in so far, as our sweet spot predominantly covered white matter areas surrounding the STN. Different tracts have been proposed to be involved in the improvement of parkinsonian symptoms, such as the hyperdirect pathway,[20,43] the lenticular fasciculus,[20,44] and direct connections between STN and the globus pallidus.[45] Tremor improvement has been linked to stimulating cerebellothalamocortical connections.[43,46] In addition, Horn et al and Akram et al showed that structural connectivity to the supplementary motor area might play an essential role in alleviating PD symptoms.[25,29]

Clinical Implications

Our study provides new functional sweet spots for different motor symptoms, which we make freely available within the Lead-DBS toolbox (https://www.lead-dbs.org/) and the Open Science Framework (https://dx.doi.org/10.17605/OSF.IO/YBDJF). With recent and upcoming DBS hardware like directional DBS leads, the sheer amount of possible stimulation settings[28] can increase the programming burden for both patients and clinicians, especially during monopolar reviews, which have long been promoted as the first programming step after implantation.[47,48] Using an independent cohort with directional leads, we could demonstrate that stimulation overlap with the sweet spot is a significant predictor for acute motor responses to DBS. Thus, visualizing a patient's DBS lead together with the functional sweet spots might be able to guide clinical DBS programming by providing a starting point for further optimization (see Fig 4B, C).[27] Furthermore, our functional sweet spot might serve as the basis for semiautomatic optimization strategies, which have been proposed for several years[16] but remain to be implemented in clinical routine. New algorithms that can optimize DBS settings almost in real time to maximize overlap with a target structure and to minimize stimulation spread into adjacent structures at some point could replace time-consuming conventional programming strategies.[49] However, our results highlight that one first needs to identify the most promising target structure and that functional sweet spots might lead to much better results than atlas-based targets like the STN. In addition to its implications for postoperative programming, one could also ask whether our sweet spot should impact surgical targeting. Although our results suggest that stimulation of the STN's surroundings is important for symptom improvement, the center of mass of the sweet spot was still positioned inside the dorsal STN. Furthermore, this point was virtually identical[5,8] or very close to[6,25] previously published sweet spots. We thus think that direct surgical targeting of the dorsal STN still is the most viable strategy. Nonlinear transformation of the mentioned sweet spots via the MNI template into individual patient space might, however, improve targeting compared to more traditional coordinate- or landmark-based approaches.

Conclusion

This study demonstrates that sweet spots determined from probabilistic stimulation mapping can predict acute and chronic DBS outcome in PD patients implanted in the STN.

Acknowledgment

We thank M. Rhyzkov from Medtronic for providing help and insights during the early stages of the project.

Author Contributions

T.A.D., J.R., M.T.B., and L.T. contributed to the design of the study; T.A.D., J.R., A.H., C.O., P.R., H.S.D., N.L., A.A.K., V.V.-V., M.T.B., and L.T. contributed to the acquisition and analysis of data; T.A.D. and J.R. contributed to drafting the text and preparing the figures. A.H., C.O., P.R., H.S.D., A.A.K., V.V.-V., G.R.F, M.T.B., and L.T. reviewed and revised the manuscript for intellectual content.

Potential Conflicts of Interest

The following authors received speaker honoraria, travel grants, and/or other funding from different commercial entities in the DBS field unrelated to this study: Medtronic (T.A.D., A.H., A.A.K, M.T.B., V.V.-V., L.T.), Boston Scientific (T.A.D., A.A.K., M.T.B., V.V.-V., L.T.), St Jude Medical/Abbot (A.A.K., V.V.-V., L.T.), Sapiens Steering Brain Stimulation (V.V.-V., L.T.).

References

1. Krack P, Martinez-Fernandez R, del Alamo M, Obeso JA. Current applications and limitations of surgical treatments for movement disorders. Mov Disord 2017;32:36–52.
2. Hamel W, Köppen JA, Alesch F, et al. Targeting of the subthalamic nucleus for deep brain stimulation: a survey among Parkinson disease specialists. World Neurosurg 2017;99:41–46.
3. Tripoliti E, Zrinzo L, Martinez-Torres I, et al. Effects of contact location and voltage amplitude on speech and movement in bilateral subthalamic nucleus deep brain stimulation. Mov Disord 2008;23:2377–2383.
4. Wodarg F, Herzog J, Reese R, et al. Stimulation site within the MRI-defined STN predicts postoperative motor outcome. Mov Disord 2012;27:874–879.
5. Horn A, Kühn AA, Merkl A, et al. Probabilistic conversion of neurosurgical DBS electrode coordinates into MNI space. Neuroimage 2017;150:395–404.
6. Bot M, Schuurman PR, Odekerken VJJ, et al. Deep brain stimulation for Parkinson's disease: defining the optimal location within the subthalamic nucleus. J Neurol Neurosurg Psychiatry 2018;89:493–498.
7. Plaha P, Ben-Shlomo Y, Patel NK, Gill SS. Stimulation of the caudal zona incerta is superior to stimulation of the subthalamic nucleus in improving contralateral parkinsonism. Brain 2006;129:1732–1747.
8. Caire F, Ranoux D, Guehl D, et al. A systematic review of studies on anatomical position of electrode contacts used for chronic subthalamic stimulation in Parkinson's disease. Acta Neurochir (Wien) 2013;155:1647–1654.
9. Mädler B, Coenen VA. Explaining clinical effects of deep brain stimulation through simplified target-specific modeling of the volume of activated tissue. Am J Neuroradiol 2012;33:1072–1080.
10. Kuncel AM, Cooper SE, Grill WM. A method to estimate the spatial extent of activation in thalamic deep brain stimulation. Clin Neurophysiol 2008;119:2148–2158.

11. Astrom M, Diczfalusy E, Martens H, Wardell K. Relationship between neural activation and electric field distribution during deep brain stimulation. IEEE Trans Biomed Eng 2015;62:664–672.

12. McIntyre CC, Mori S, Sherman DL, et al. Electric field and stimulating influence generated by deep brain stimulation of the subthalamic nucleus. Clin Neurophysiol 2004;115:589–595.

13. Chaturvedi A, Luján JL, McIntyre CC. Artificial neural network based characterization of the volume of tissue activated during deep brain stimulation. J Neural Eng 2013;10:056023.

14. Astrom M, Tripoliti E, Hariz MI, et al. Patient-specific model-based investigation of speech intelligibility and movement during deep brain stimulation. Stereotact Funct Neurosurg 2010;88:224–233.

15. Maks CB, Butson CR, Walter BL, et al. Deep brain stimulation activation volumes and their association with neurophysiological mapping and therapeutic outcomes. J Neurol Neurosurg Psychiatry 2009;80: 659–666.

16. Frankemolle AMM, Wu J, Noecker AM, et al. Reversing cognitive-motor impairments in Parkinson's disease patients using a computational modelling approach to deep brain stimulation programming. Brain 2010;133:746–761.

17. Mikos A, Bowers D, Noecker AM, et al. Patient-specific analysis of the relationship between the volume of tissue activated during DBS and verbal fluency. Neuroimage 2011;54(suppl 1):S238–S246.

18. Eisenstein SA, Koller JM, Black KD, et al. Functional anatomy of subthalamic nucleus stimulation in Parkinson disease. Ann Neurol 2014; 76:279–295.

19. Gourisankar A, Eisenstein SA, Trapp NT, et al. Mapping movement, mood, motivation and mentation in the subthalamic nucleus. R Soc Open Sci 2018;5:171177.

20. Butson CR, Cooper SE, Henderson JM, et al. Probabilistic analysis of activation volumes generated during deep brain stimulation. Neuroimage 2011;54:2096–2104.

21. Dembek TA, Barbe MT, Åström M, et al. Probabilistic mapping of deep brain stimulation effects in essential tremor. Neuroimage Clin 2017;13:164–173.

22. Cheung T, Noecker AM, Alterman RL, et al. Defining a therapeutic target for pallidal deep brain stimulation for dystonia. Ann Neurol 2014;76:22–30.

23. Phibbs FT, Pallavaram S, Tolleson C, et al. Use of efficacy probability maps for the post-operative programming of deep brain stimulation in essential tremor. Parkinsonism Relat Disord 2014;20:1341–1344.

24. Fytagoridis A, Åström M, Samuelsson J, Blomstedt P. Deep brain stimulation of the caudal zona incerta: tremor control in relation to the location of stimulation fields. Stereotact Funct Neurosurg 2016; 94:363–370.

25. Akram H, Sotiropoulos SN, Jbabdi S, et al. Subthalamic deep brain stimulation sweet spots and hyperdirect cortical connectivity in Parkinson's disease. Neuroimage 2017;158:332–345.

26. Reich MM, Horn A, Lange F, et al. Probabilistic mapping of the antidystonic effect of pallidal neurostimulation: a multicentre imaging study. Brain 2019;142:1386–1398.

27. Butson CR, Tamm G, Jain S, et al. Evaluation of interactive visualization on mobile computing platforms for selection of deep brain stimulation parameters. IEEE Trans Vis Comput Graph 2013;19: 108–117.

28. Dembek TA, Reker P, Visser-Vandewalle V, et al. Directional DBS increases side-effect thresholds—a prospective, double-blind trial. Mov Disord 2017;32:1380–1388.

29. Horn A, Reich M, Vorwerk J, et al. Connectivity predicts deep brain stimulation outcome in Parkinson disease. Ann Neurol 2017;82:67–78.

30. Horn A, Li N, Dembek TA, et al. Lead-DBS v2: towards a comprehensive pipeline for deep brain stimulation imaging. Neuroimage 2019;184:293–316.

31. Avants BB, Epstein CL, Grossman M, Gee JC. Symmetric diffeomorphic image registration with cross-correlation: evaluating automated labeling of elderly and neurodegenerative brain. Med Image Anal 2008;12:26–41.

32. Schönecker T, Kupsch A, Kühn AA, et al. Automated optimization of subcortical cerebral MR imaging-atlas coregistration for improved postoperative electrode localization in deep brain stimulation. AJNR Am J Neuroradiol 2009;30:1914–1921.

33. Fonov V, Evans AC, Botteron K, et al. Unbiased average age-appropriate atlases for pediatric studies. Neuroimage 2011;54:313–327.

34. Husch A, V Petersen M, Gemmar P, et al. PaCER—a fully automated method for electrode trajectory and contact reconstruction in deep brain stimulation. Neuroimage Clin 2017;17:80–89.

35. Sitz A, Hoevels M, Hellerbach A, et al. Determining the orientation angle of directional leads for deep brain stimulation using computed tomography and digital x-ray imaging: a phantom study. Med Phys 2017;44:4463–4473.

36. Ewert S, Plettig P, Li N, et al. Toward defining deep brain stimulation targets in MNI space: a subcortical atlas based on multimodal MRI, histology and structural connectivity. Neuroimage 2018;170:271–282.

37. Burnham KP, Anderson DR. Multimodel inference: understanding AIC and BIC in model selection. Sociol Methods Res 2004;33:261–304.

38. Nestor KA, Jones JD, Butson CR, et al. Coordinate-based lead location does not predict Parkinson's disease deep brain stimulation outcome. PLoS One 2014;9:e93524.

39. Åström M, Lemaire J-J, Wårdell K. Influence of heterogeneous and anisotropic tissue conductivity on electric field distribution in deep brain stimulation. Med Biol Eng Comput 2011;50:23–32.

40. Chaturvedi A, Butson CR, Lempka SF, et al. Patient-specific models of deep brain stimulation: influence of field model complexity on neural activation predictions. Brain Stimul 2010;3:65–67.

41. Gunalan K, Chaturvedi A, Howell B, et al. Creating and parameterizing patient-specific deep brain stimulation pathway-activation models using the hyperdirect pathway as an example. PLoS One 2017;12:e0176132.

42. Sweet JA, Pace J, Girgis F, Miller JP. Computational modeling and neuroimaging techniques for targeting during deep brain stimulation. Front Neuroanat 2016;10:71.

43. Avecillas-Chasin JM, Alonso-Frech F, Parras O, et al. Assessment of a method to determine deep brain stimulation targets using deterministic tractography in a navigation system. Neurosurg Rev 2015;38:739–751.

44. Miocinovic S, Parent M, Butson CR, et al. Computational analysis of subthalamic nucleus and lenticular fasciculus activation during therapeutic deep brain stimulation. J Neurophysiol 2006;96:1569–1580.

45. Pujol S, Cabeen R, Sébille SB, et al. In vivo exploration of the connectivity between the subthalamic nucleus and the globus pallidus in the human brain using multi-fiber tractography. Front Neuroanat 2017;10:119.

46. Coenen VA, Allert N, Paus S, et al. Modulation of the cerebello-thalamo-cortical network in thalamic deep brain stimulation for tremor: a diffusion tensor imaging study. Neurosurgery 2014;75:657–670.

47. Picillo M, Lozano AM, Kou N, et al. Programming deep brain stimulation for Parkinson's disease: the Toronto Western Hospital algorithms. Brain Stimul 2016;9:425–437.

48. Volkmann J, Herzog J, Kopper F, Deuschl G. Introduction to the programming of deep brain stimulators. Mov Disord 2002;17(suppl 3):S181–S187.

49. Anderson DN, Osting B, Vorwerk J, et al. Optimized programming algorithm for cylindrical and directional deep brain stimulation electrodes. J Neural Eng 2018;15:026005.